Ceramics International xxx (xxxx) xxx–xxx

Contents lists available at ScienceDirect

Ceramics International

journal homepage: www.elsevier.com/locate/ceramint

Cation distribution of high-performance Mn-substituted $ZnGa_2O_4$ microwave dielectric ceramics

Xiaochi Lu[a,b], Wenjie Bian[a,b], Chengfa Min[a,b], Zhenxiao Fu[c], Qitu Zhang[a,b,*], Haikui Zhu[a,b,*]

[a] College of Materials Science and Engineering, Nanjing Tech University, Nanjing 210009, PR China
[b] Jiangsu Collaborative Innovation Center for Advanced Inorganic Function Composites, Nanjing Tech University, Nanjing 210009, PR China
[c] State Key Laboratory of Advanced Materials and Electronic Components, Guangdong Fenghua Advanced Technology Holding Co., Ltd, Zhaoqing 526020, PR China

ARTICLE INFO

Keywords:
$ZnGa_2O_4$ ceramic
Mn-substitution
Spinel
Dielectric properties
Cation distribution

ABSTRACT

In current study, only 5 mol% Mn^{2+} was applied to fabricate high performance microwave dielectric $ZnGa_2O_4$ ceramics, via a traditional solid state method. The crystal structure, cation distribution and microwave dielectric properties of as-fabricated Mn-substituted $ZnGa_2O_4$ ceramics were systematically investigated. Mn^{2+}-substitution led to a continuous lattice expansion. Raman, EPR and crystal structure refinement analysis suggest that Mn^{2+} preferentially occupies the tetrahedral site and the compounds stay normal-spinel structure. The experimental and theoretical dielectric constant of $Zn_{1-x}Mn_xGa_2O_4$ ceramics fit well. In all, this magnetic ion, Mn^{2+}, could effectively adjust the τ_f value to near zero and double the quality factor from 85,824 GHz to 181,000 GHz of $Zn_{1-x}Mn_xGa_2O_4$ ceramics at the meantime. $Zn_{1-x}Mn_xGa_2O_4$ ($x = 0.05$) ceramics sintered at 1400 °C for 2 h exhibited excellent microwave dielectric properties, with $\varepsilon_r = 9.7$(@9.85 GHz), $Q \times f = 181{,}000$ GHz, $tan\delta = 5.44 \times 10^{-5}$,and $\tau_f = -12$ ppm/°C.

1. Introduction

Low-K microwave dielectric ceramic materials have long been studied as millimeter wireless communication systems [1–5]. It is required to possess low dielectric constant , high quality factor and near zero temperature coefficient, so that these materials can widen the wave width, utilize frequency resource sufficiently, and shorten the relaxation time. And it is crucial to advancing the properties of intelligent transport systems, excellent ultra-stable oscillators, and ultrahigh-speed wireless local area networks.

Spinel compounds, one of the typical low-K dielectric ceramic materials, with general formula AB_2O_4 or $B(AB)O_4$, is applied in many scientific and commercial fields, such as magnetic materials, catalysts, semiconductors, superconductors and microwave dielectric ceramics. Common spinel ceramics for millimeter region application include M_2SnO_4 [6–8] M_2SiO_4 [9–11] and MAl_2O_4 [12–15] (M = Zn, Mg). Compared with M_2SnO_4, M_2SiO_4 and MAl_2O_4 (M = Zn, Mg), MGa_2O_4 (M = Zn, Mg) [16–23] have high quality factors over 90,000 GHz, low sintering temperature and a wide sintering temperature region. Therefore, MGa_2O_4 (M = Zn, Mg) spinel materials are promising candidates for millimeter-wave region application. However , the crystal structure of these two spinel ceramics are different. The crystal structure of $ZnGa_2O_4$ and MGa_2O_4 are normal-spinel and partial normal-spinel, respectively.

Researches have been studied the dielectric performance of $ZnGa_2O_4$ [16–18], $MgGa_2O_4$ [19,20] and their solid solutions, such as (Zn, Mg)Ga_2O_4 [21] and Zn (Ga, Al)$_2O_4$ [22]. These compounds are all spinel structured ceramics, and researchers believed that cation distribution play an important role in the enhancement of the $Q \times f$ value. Crystal structure refinement was applied to clarify the relationship between the crystal structure and the microwave dielectric properties of $MgGa_2O_4$. Akinori Kan etc. use crystal structure refinement to investigate $MgGa_2O_4$ spinel materials [20]. In their research, although the relative density is the same value of about 96%, $MgGa_2O_4$ ceramics with 0.86° of inversion show greater microwave dielectric performance than samples with higher (0.88) or lower (0.84) inversion parameter. Takahashi [23] investigated the cation distribution of spinel-structured $Zn_{1-3x}Al_{2+2x}O_4$ (x = 0–0.2) ceramics with defective structures and found that an intermediate spinel structure with preferential occupancy of tetrahedral sites by trivalent cations exhibits an enhanced $Q \times f$ value.

In the case of $ZnGa_2O_4$, fewer studies investigated the relationship between the cation distribution and the microwave dielectric properties. In our previous research, appropriate Cu-substitution can promote the microwave dielectric performance of $ZnGa_2O_4$, especially the $Q \times f$ value which climbed from 85,824 GHz to 131,445 GHz. Moreover, both

* Corresponding authors at: College of Materials Science and Engineering, Nanjing Tech University, Nanjing 210009, PR China.
E-mail addresses: ngdzqt@163.com (Q. Zhang), zhk@njtech.edu.cn (H. Zhu).

https://doi.org/10.1016/j.ceramint.2018.02.041
Received 19 January 2018; Received in revised form 1 February 2018; Accepted 4 February 2018

the Raman spectrometer analysis and the crystal structure refinement demonstrate that the preferential site occupancy of Cu^{2+} is the octahedral site [24].

The above investigations were mainly focused on improving the quality factor of spinel structured ceramics, especially the gallium compounds. However, in the case of $ZnGa_2O_4$ microwave dielectric ceramic, the larger negative τ_f value, ~ -60 ppm/°C, has limited its application for millimeter-wave region. Therefore, it is significant to tune its τ_f value to near zero. Usually, these following two ways, substitution with magnetic ion and introducing second phase with positive τ_f value, are widely accepted to shift the large negative τ_f value to near zero [25]. Although introducing second phase with positive τ_f value could adjust the τ_f value to near zero, the $Q \times f$ value always be decreased in the meanwhile. Therefore, almost all of the commercial microwave dielectric products on the market today tune τ_f through the addition of varying amounts of magnetic additives, such as Ni, Co, and Mn, for magnetic additives could promote the $Q \times f$ value at the same time. Therefore, it came to us that whether or not can magnetic additives adjust the τ_f value to near zero and improve other dielectric performance at the same time.

Thus, in this paper Mn was introduced at the level of x = 0, 0.01, 0.05, 0.1 and 0.15, the effects of the preferential site occupation and magnetic ion Mn role on the microwave dielectric properties were investigated.

2. Materials and methods

2.1. Powder synthesis

$Zn_{1-x}Mn_xGa_2O_4$ (x = 0–0.15) spinel ceramics were prepared via traditional solid state method. ZnO, $MnCO_3$, and Ga_2O_3 powders were selected as the starting material. Analytical grade powders were weighted precisely using an analytical balance on the basis of stoichiometric proportions, to form a $Zn_{1-x}Mn_xGa_2O_4$ (x = 0–0.15) formula in the resultant Mn-substituted $ZnGa_2O_4$ spinel solid solutions. The substitution amount of $MnCO_3$ in this work was employed as 0.00 mol %, 0.01 mol%, 0.05 mol%, 0.10 mol%, 0.15 mol%, denoted as ZGO, 1ZMGO, 5ZMGO, 5ZMGO and 15ZMGO, respectively.

The mixed powders were milled for 12 h with ethanol in polyethylene jars with agate balls in a planetary milling machine (QM-1SP4; Jialing, Nanjing, China) with a rotation speed of 300 rpm. The obtained slurry was dried at 100 °C in an oven for 24 h in air, followed by sieved though a 100 mesh screen. The sieved powders were mixed with 7 wt% polyvinyl alcohol as adhesion agent and pressed into pellets of 13 mm in diameter and 6 mm in thickness with an automatic machine (DY-20; Tianjin Keqi Instrument, Tianjin, China) under 75 MPa. The green bodies were calcined at 1000 °C for 3 h in air to remove the volatile impurities in a muffle furnace and form the solid solutions. After calcining, the pellets were sintered at 1250–1350 °C for 4 h in air with a high-temperature electric furnace (KSX4-16, Allfine, Wuxi, China). Densities of the ceramics were evaluated via the Archimedes method and 5 samples were measured for every sintering temperature and give the average density. The relative densities were obtained based on bulk and theoretical density. Microstructural evolution of obtained ceramics was investigated by a scanning electron microscope (SEM, Hitachi SU8010, Japan).

2.2. Structure analysis

The XRD profiles of the ceramics were obtained by a step scanning method in the 2θ range of 5–80° with a step size of 0.02° and a counting time of 3.0 s/step, using X-ray diffraction (XRD, RigakuD/Max 2500 type, Japan) with Cu Kα radiation. Raman spectra were excited with an argon laser (20 mW laser power) and recorded using a Raman spectrometer (HR800, Horiba Labram, 514 nm He-Cd laser, 20 mW laser power). The manganese oxidation state and its position in the Mn-doped spinel structure were examined with EPR spectroscopy. It was carried out with standard X-band EPR spectrometer at a frequency of 9.7 GH (Bruker Elexsys FT/CW 580). The effect of Mn substitution on the crystal structure was investigated with General Structure Analysis System (PC-GSAS) software. Fourier transform infrared (FT-IR) spectroscopy was performed by NICOLET 5700 (Thermo, America).

2.3. Dielectric performance analysis

To investigate the microwave dielectric performance, ε_r, $Q \times f$, f_0 and τ_f were detected using cavity resonator method [26] by using Lightwave Component Analyzer (Hewlett Packard 8703 A, 1550 nm/130 MHz–20 GHz) and the resonator size is ϕ36 mm × h25 mm. The temperature coefficient of resonant frequency (τ_f) was calculated in the temperature range from 20 °C to 90 °C.

3. Results and discussion

3.1. Phase composition and sintering behavior

The spinel structured Mn-substituted $ZnGa_2O_4$ ceramics have been analyzed by XRD patterns (shown in Fig. 1). Obviously, all the diffraction peaks could be well indexed to spinel structured $ZnGa_2O_4$ (JCPDS No.86-0413) or $MnGa_2O_4$ (JCDPS No. 72-1521) with the space group *Fd3m*, and no $ZnMn_2O_4$ phase ((JCDPS No.77-0470, space group *I*41/*amd*) was detected in these specimen. $ZnGa_2O_4$ and $MnGa_2O_4$ both belong to normal spinel compounds. Notably, the reflection of $Zn_{1-x}Mn_xGa_2O_4$ shifted significantly to lower diffraction angles as *x* increased, especially the main diffraction peaks (shown in Fig. 1b). The reflections shift could be ascribed to the lattice expansion.

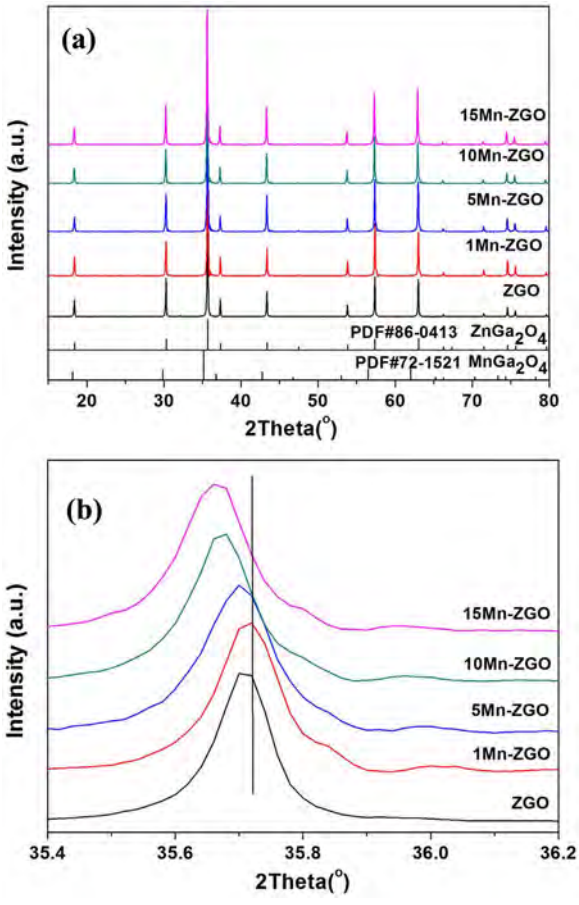

Fig. 1. XRD patterns (a) and their enlarged XRD patterns (b) of $Zn_{1-x}Mn_xGa_2O_4$ (x = 0–0.15) ceramics sintered at 1400 °C for 2 h in air.

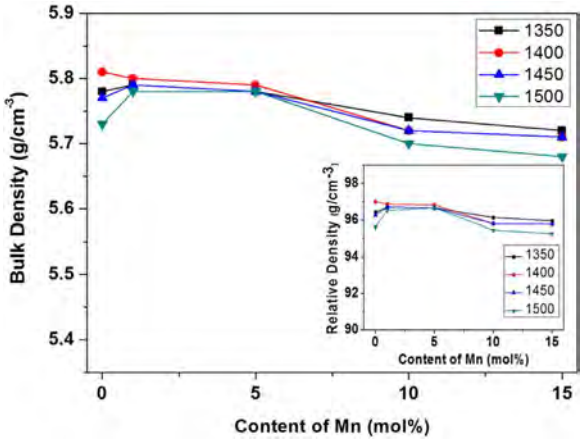

Fig. 2. The bulk densities and the relative densities of $Zn_{1-x}Cu_xGa_2O_4$ (x = 0–0.15) ceramics, sintered at various temperatures range from 1350 °C to 1500 °C for 2 h in air.

The densities of $Zn_{1-x}Mn_xGa_2O_4$ (x = 0–0.15) are offered in Fig. 2. For each composition, the bulk densities initially climbed with increasing sintering temperature, and then decreased after reaching a maximum value. The lower bulk density of $MnGa_2O_4$ (5.80 g/cm^3) than $ZnGa_2O_4$ (5.99 g/cm^3) may take account for the decrease. With a small amount of Mn-substitution, the maximum bulk densities increased and the relative densities climbed with Mn content (1% and 5%), exhibited in the insert image. This indicated that partial Mn-substitution could promote the densification of $ZnGa_2O_4$ ceramics. And the optimal sintering temperature of samples at which the maximum densities were obtained is 1400 °C.

SEM micrographs of $Zn_{1-x}Mn_xGa_2O_4$ ceramics with various Mn^{2+} content sintered at 1400 °C are exhibited in Fig. 3. The average grain size increased with Mn content. And at the range from 0 to 0.1, the average grain size increased slightly. When substituted with 15 mol% Mn (shown in Fig. 3e), the grain size increased a lot, properly due to the movement of the grain boundaries through consuming smaller grains. In general, Mn-substitution interact the microstructure of $ZnGa_2O_4$ weakly. Therefore, it can also conclude that the role of Mn ion is not the sintering add but the substitution.

3.2. Cation distribution and crystal structure

The distribution of cations can be suggested by the data of Raman spectroscopy. Fig. 4 displays the Raman profiles of Mn^{2+} substituted $ZnGa_2O_4$ ceramics, recorded at room temperature. The Raman spectra of $Zn_{1-x}Mn_xGa_2O_4$ consists of three distinct peaks at around 468 (T_{2g}), 607 (T_{2g}), and 712 (A_{1g}) which are consistent with the Rafal Wglusz's research [27]. In our previous research, the presence of extra band associated with A_{1g} mode, marked with A^*_{1g}, can be connected to the site inversion and has informative value for the direct recognition of an inverted spinel [24,28]. Therefore, Mn-substituted $ZnGa_2O_4$ solid solution is still a normal spinel compound. In other words, Mn ion substituted Zn ion on tetrahedral site in $Zn_{1-x}Mn_xGa_2O_4$ ceramics.

Fig. 5 shows the EPR spectrum of 5ZMGO recorded at RT. The EPR data exhibit six-line ($\Delta m_S = \pm 1$, $\Delta m_I = 0$) patterns around g = 2.0044, which according to Singh [29] indicated Mn^{2+} were in an axial symmetry sites. Furthermore, no weak forbidden hyperfine lines were observed. In fact, forbidden hyperfine lines indicates on some distortion that lowers the symmetry of cubic structure and supports the location of Mn^{2+} on octahedral site [30,31]. Hence, EPR analysis certified that Mn oxidation states is Mn^{2+} located on the tetrahedral site in $Zn_{1-x}Mn_xGa_2O_4$ spinel structure.

Rietveld refinement was used to analyze the structure evolution in the Mn-substituted $ZnGa_2O_4$ ceramic system. In fact, the octahedral site preference energy (OSPE) of Mn^{2+} and Zn^{2+} is 0 kcal/mol, hence Mn^{2+} and Zn^{2+} prefer to occupy the tetrahedral site than octahedral site in the structure of $ZnGa_2O_4$ spinel. Therefore, XRD refinement was carried out on the basis of previous XRD, Raman and EPR analysis, as well as crystal field theory. The refinement involved lattice parameters, background, atomic coordinates, site occupancies and isotropic thermal parameters.

A part of the refinement analysis for Mn-substituted $ZnGa_2O_4$ such as lattice parameters are exhibited in Fig. 6a. From the refinement results, it was found that there was an expansion in the lattice parameter with Mn-substitution, which confirmed the previous XRD analysis. The lattice parameter, a, shows a significant linear correlation with Mn content. This indicates that $Zn_{1-x}Mn_xGa_2O_4$ is a solid solution and the limit of Mn^{2+} solubility in the $ZnGa_2O_4$ is above 15%. Therefore, the $MnCO_3$ is not an aid, but doping into the crystalline structure of $ZnGa_2O_4$, exhibited in Fig. 6b.

Table 1 summarizes the refine atomic coordinates, atomic occupancies, and reliability factors (R_{wp} and R_p) of $Zn_{1-x}Mn_xGa_2O_4$ (x = 0–0.15) ceramics sintered at 1400 °C for 2 h. The crystal structures were refined to clarify the relationship between the cation distribution and Mn content. The crystal structure parameters of $ZnGa_2O_4$ (JCPDS No.86-0413) were applied as the initial parameters for refinement of the crystal structure of the $Zn_{1-x}Mn_xGa_2O_4$ (x = 0–0.15) ceramics. The results indicated that Mn^{2+} cation preferentially occupies the tetrahedral site with Zn^{2+} (see Fig. 5b), which correspond to the prediction we made.

FT-IR spectrum of $Zn_{1-x}Mn_xGa_2O_4$ (x = 0–0.05) ceramics sintered at 1400 °C for 2 h were displayed in Fig. 7. The absorption peaks at around 577 cm^{-1} and 434 cm^{-1} represent the bond vibration of Zn-O-Ga and Zn-O. The shift of absorption bands in FT-IR spectrum is due to Mn-substitution. Based on the refined crystal structure and Raman spectrum data, Mn cation preferentially occupies the tetrahedral site. Therefore Zn–O–Ga and Zn–O bonds were partially substituted by Mn–O–Ga and Mn–O. The higher ion radii of Mn^{2+} (CN = 4, r = 0.66) than Zn^{2+} (CN = 4, r = 0.6) resulted in weaker bond strength, and the absorption peak at around 434 cm^{-1} ultimately shifted to higher wavenumber from 432 cm^{-1} to 440 cm^{-1}. The expansion of cell parameters may take responsibilities for the shift of 573 cm^{-1} absorption peak. Therefore, the FT-IR spectrum data could in turn confirm the analysis of refined XRD and Raman spectrum of $Zn_{1-x}Mn_xGa_2O_4$ (x = 0–0.05) ceramics.

3.3. Microwave dielectric properties

Table 2 shows the compositions, ε_r, f_0, $Q \times f$, and τ_f values for the ceramics prepared in this study. $Zn_{1-x}Mn_xGa_2O_4$ shows promising dielectric properties (ε_r = 9.7, $Q \times f$ = 181,000 @ 9.85 GHz).

Fig. 8a shows the ion polarizabilities (α_m) and molecular volumes (V_m) of Mn-substituted $Zn_{1-x}Mn_xGa_2O_4$ ceramics. These data were based on two assumptions that $Zn_{1-x}Mn_xGa_2O_4$ ceramics were dense and could be used in particle fields. The α_m of ZnO, MnO and Ga_2O_3 are 4.01, 4.46 and 8.96, respectively [32]. Therefore, the total dielectric polarizability $\alpha_m = (1\text{-}x)^*\alpha(ZnO) + x^*\alpha(MnO) + \alpha(Ga_2O_3)$. And the Vm data were obtained based on the refinement analysis. Notably, both ion polarizability (α_m) and molecular volume (V_m) exhibited a strong linear positive correlation with the climbing Mn-substitution (shown in Fig. 8a).

The theoretical dielectric constant, shown in Fig. 7b, were obtained using the Clausius-Mosotti Eq. (1)

$$\varepsilon_r = [3/(1 - b\alpha_m/Vm)] - 2 \quad (1)$$

Vm and α_m were mentioned above, and b is a constant which is equal to $4\pi/3$. The theoretical ε_r varied as Mn content climbed. Because Vm is the denominator, α_m is the numerator, both of them have a positive relation with Mn content, and the slopes of Vm and α_m are almost the same-hence α_m/Vm varied around a constant and so were the ε_r (~ 10). The experimental ε_r of $Zn_{1-x}Mn_xGa_2O_4$ show a similar trend as the

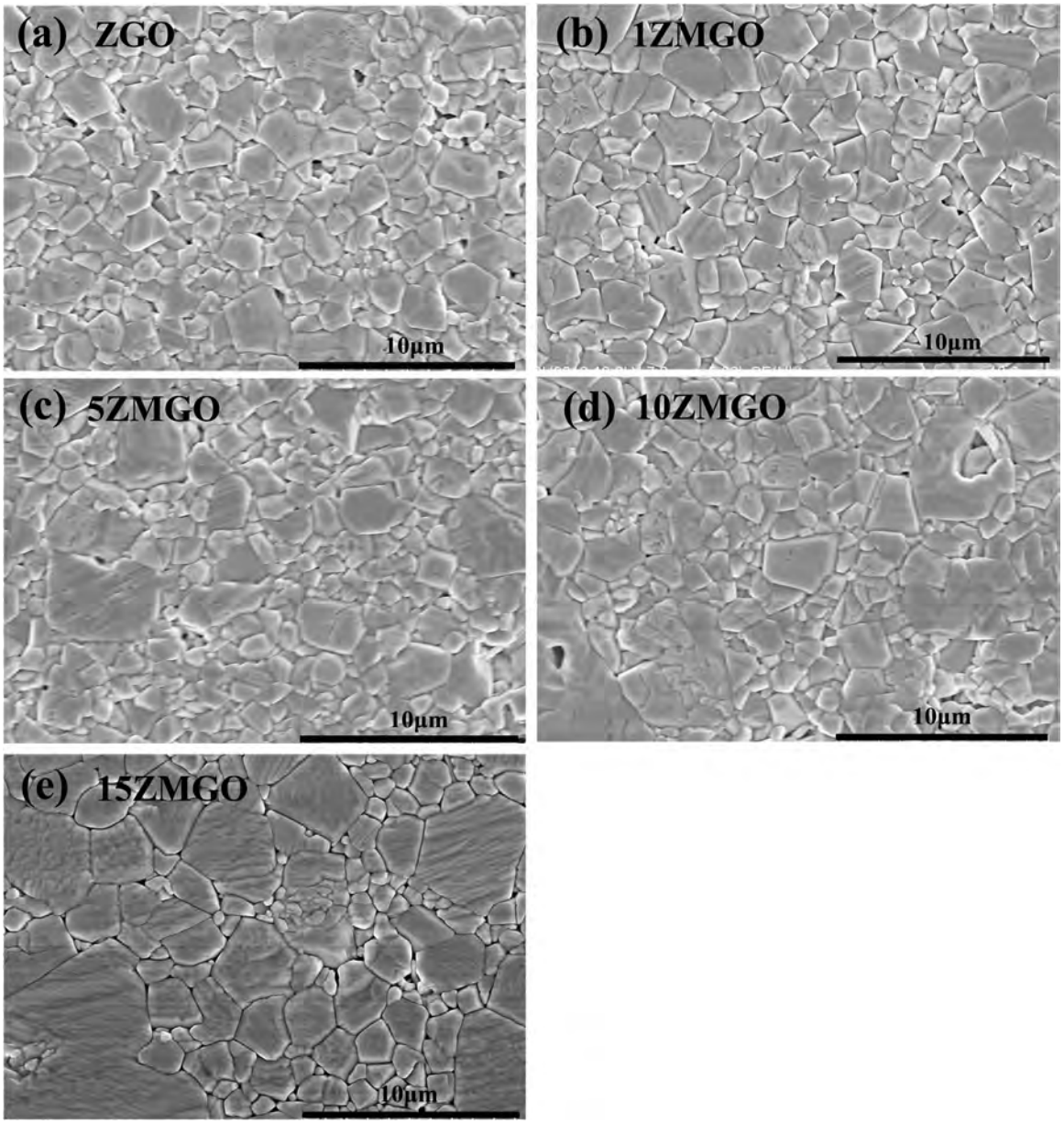

Fig. 3. SEM images of thermal etched surface of Zn1-xMnxGa$_2$O$_4$ (x = 0–0.15) ceramics sintered at 1400 °C for 2 h in air: (a) x = 0; (b) x = 0.01; (c) x = 0.05; (d-e) x = 0.1; (f) x = 0.15, respectively.

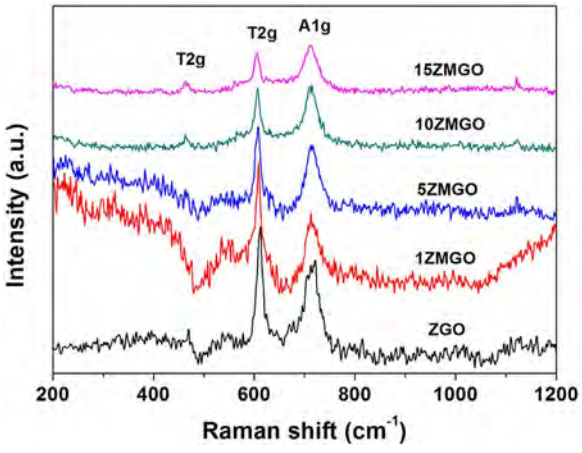

Fig. 4. Raman spectra of $Zn_{1-x}Mn_xGa_2O_4$ (x = 0–0.15), sintered at 1400 °C for 2 h in air.

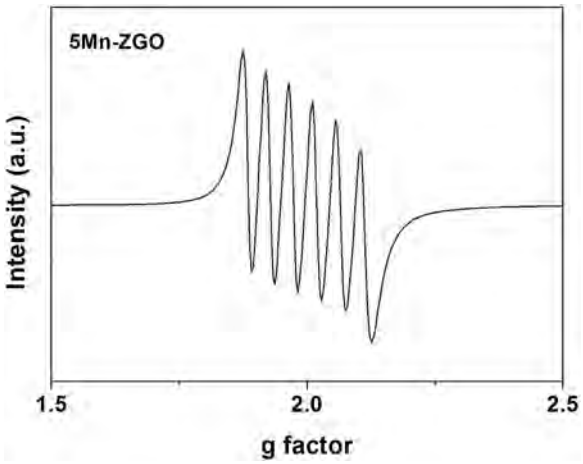

Fig. 5. EPR spectrum of $Zn_{0.95}Mn_{0.05}Ga_2O_4$, sintered at 1400 °C for 2 h in air.

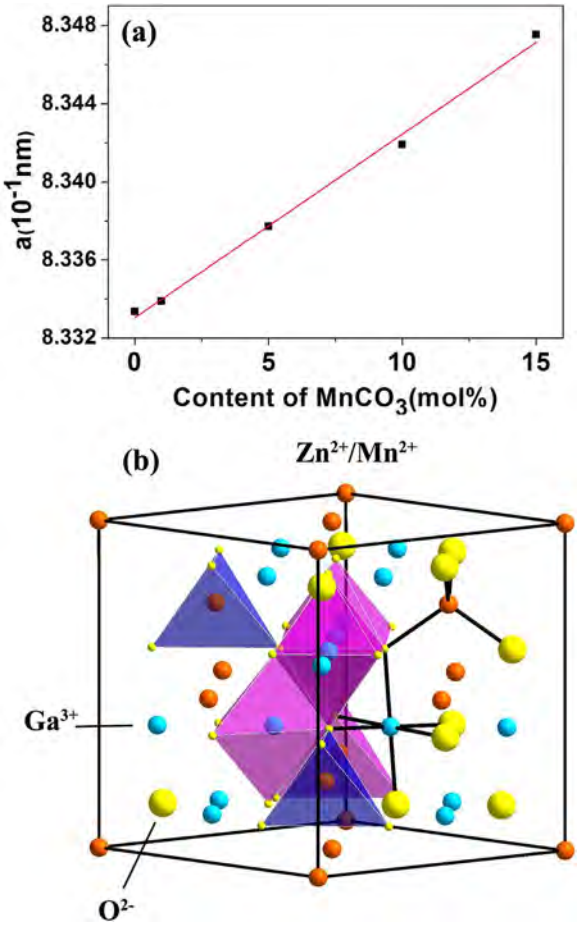

Fig. 6. (a) Refined cell parameters a and (b) crystal structure of $Zn_{1-x}Cu_xGa_2O_4$ fired at 1400 °C for 2 h in air.

Table 1
Refined crystal structure parameters of $Zn_{1-x}Mn_xGa_2O_4$ fired at 1400 °C for 2 h.

Content of Mn (mol %)%	Atom	Site	Site occupancy	Atomic coordinates		
				x	y	z
0						
W_{Rp} = 9.29%	Zn^{2+}	8a	1	0.125	0.125	0.125
R_p = 6.71%	Ga^{3+}	16d	1	0.5	0.5	0.5
	O	32e	1	0.2631	0.2631	0.2631
0.01						
W_{Rp} = 12.61%	Zn^{2+}/ Mn^{2+}	8a	0.99/0.01	0.125	0.125	0.125
R_p = 9.52%	Ga^{3+}	16d	1	0.5	0.5	0.5
	O	32e	1	0.261	0.261	0.2621
0.05						
W_{Rp} = 12.8%	Zn^{2+}/ Mn^{2+}	8a	0.94/0.06	0.125	0.125	0.125
R_p = 9.6%	Ga^{3+}	16d	1	0.5	0.5	0.5
	O	32e	1	0.262	0.262	0.262
0.1						
W_{Rp} = 13.5%	Zn^{2+}/ Mn^{2+}	8a	0.9/0.1	0.125	0.125	0.125
R_p = 10.1%	Ga^{3+}	16d	1	0.5	0.5	0.5
	O	32e	1	0.2619	0.2619	0.2622
0.15						
W_{Rp} = 11.7%	Zn^{2+}/ Mn^{2+}	8a	0.86/0.14	0.125	0.125	0.125
R_p = 9.16%	Ga^{3+}	16d	1	0.5	0.5	0.5
	O	32e	1	0.2614	0.2614	0.2614

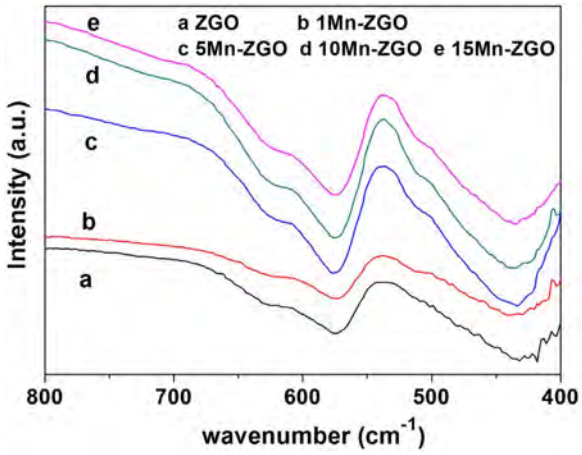

Fig. 7. FT-IR spectrum of $Zn_{1-x}Mn_xGa_2O_4$ (x = 0–0.05) ceramics, sintered at temperatures range from 1350 °C to 1500 °C for 2 h in air.

Table 2
Microwave dielectric properties of $Zn_{1-x}Mn_xGa_2O_4$ fired at 1400 °C for 2 h.

Component	ε_r	f_0 (GHz)	$Q \times f$ (GHz)	$tan\delta$ (*10^{-5})
0ZMGO	9.77	9.02	85,824	10.51
1ZMGO	9.72	9.99	118,000	8.47
5ZMGO	9.7	9.85	181,000	5.44
10ZMGO	9.67	9.79	148,000	6.61
15ZMGO	9.68	9.72	129,000	7.53

theoretical ε_r. The relative density maybe responsible for the difference between theoretical and experimental ε_r value displayed in Fig. 7b.

Fig. 8c displays $Q \times f$ values of $Zn_{1-x}Mn_xGa_2O_4$ (x = 0–0.15) sintered at temperatures from 1300 °C to 1500 °C. For each sintering temperatures, the $Q \times f$ values of $Zn_{1-x}Mn_xGa_2O_4$ (x = 0.15) are quite low (< 90,000 GHz). As is discussed in density section (Fig. 3), 1400 °C is the optimized sintering temperature for the highest bulk density and $Q \times f$ values. The $Q \times f$ values of $Zn_{1-x}Mn_xGa_2O_4$ ceramics jumped with Mn increased, to a maximum value of 181,000 GHz (x = 0.05) and then declined.

Many factors affect the $Q \times f$ values such as crystal structure, bulk density, microstructure, and secondary phase etc. In general, appropriate crystal structure, and uniform dense grain microstructure produce a tangible contribution to a high $Q \times f$ value. The crystal structure analysis suggests that Mn^{2+} cation preferentially occupies the tetrahedral site in $Zn_{1-x}Mn_xGa_2O_4$ solid solution. The preferential site occupancy of Mn^{2+} may enhance the sintering ability of $Zn_{1-x}Mn_xGa_2O_4$ ceramics, which is related to the improvement of crystallinity, lead to a rising in the microwave dielectric properties, especially $Q \times f$ value.

In the work, the improvement of $Q \times f$ value in $Zn_{1-x}Mn_xGa_2O_4$ ceramics, for instance, $Q \times f$ value increased from 85,824 GHz (x = 0) to 181,000 GHz (x = 0.05) sintered at 1400 °C, was considered as the consequence of synergistic effect among Mn^{2+} substitution, uniform microstructure, and high relative densities.

The τ_f value shows a significant improvement of Mn-substituted $ZnGa_2O_4$. As is shown in Fig. 8d, $ZnGa_2O_4$ have a large negative τ_f value ~ − 70 ppm/°C which limits its application, however, with tiny Mn-substitution, the τ_f value sharply increased to near zero ~ − 10 ppm/°C and it can be acceptable for millimeter-wave use. Furthermore, τ_f value of $Zn_{1-x}Mn_xGa_2O_4$ kept steady with continuous Mn-substitution. The factors that affect τ_f values are very complicated. Usually, τ_f value depends on the composition, relative densities, crystal structure and so on. Because the relative densities are close for $Zn_{1-x}Mn_xGa_2O_4$ and the τ_f value are stable ~ 10 ppm/°C during Mn-substitution from 0.01 to 0.15, therefore crystal structure may play a critical role in promoting τ_f properties. These results confirmed that substitution with Mn^{2+}, a

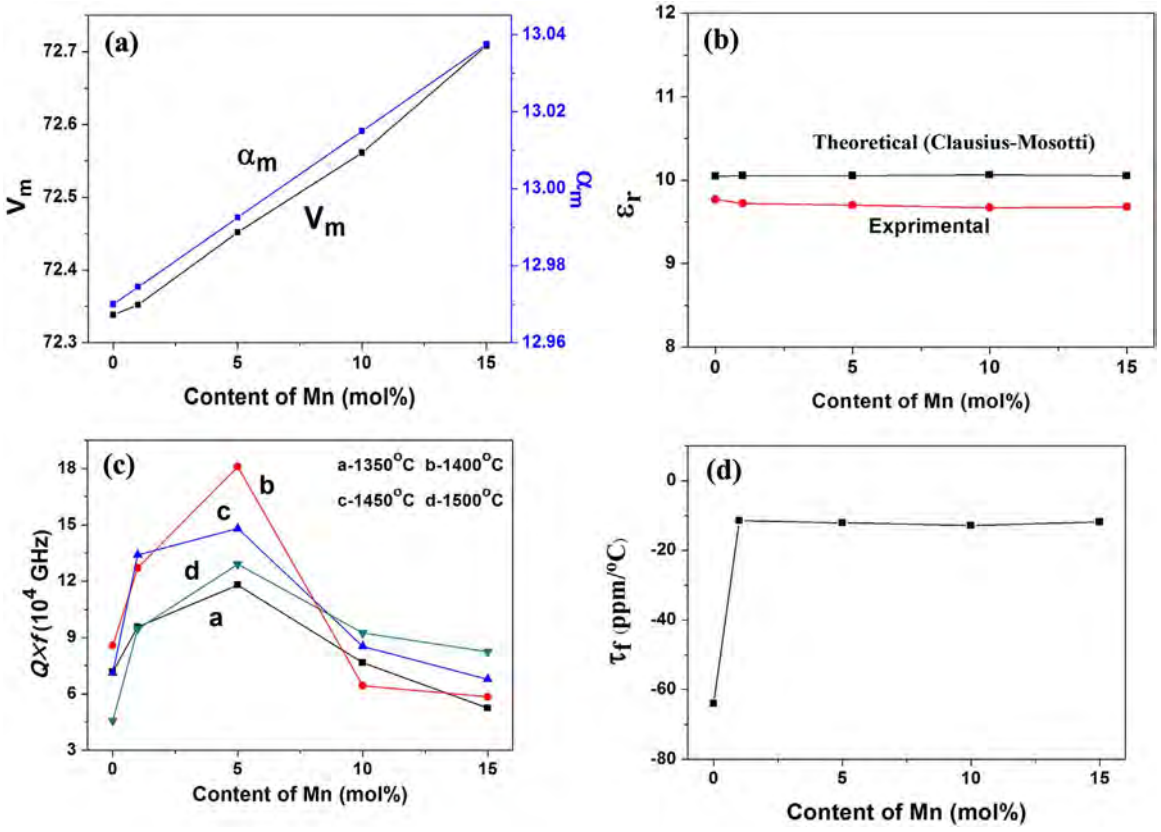

Fig. 8. Microwave dielectric properties of Mn-substituted $ZnGa_2O_4$ (a) ionic polarization and cell volume; (b) Experimental and theoretical dielectric constant; (c) $Q \times f$ values; (d) τ_f values.

magnetic ion, could effectively adjust the τ_f value of $ZnGa_2O_4$ ceramics to near zero.

4. Conclusions

In this work, a successful fabrication of high-performance $ZnGa_2O_4$ ceramics was reported. This was achieved by employing a simple solid state method using $MnCO_3$ to adjust the crystalline structure. EPR, Raman and XRD refinement all illustrated that Mn^{2+} substituted Zn^{2+} in the tetrahedral site. The experimental dielectric constant is consistent with the theoretical dielectric constant of $Zn_{1-x}Mn_xGa_2O_4$ ceramics. The preferential site occupancy of Mn^{2+}, and high relative densities leads to the high $Q \times f$ values. The $Q \times f$ value was 181,000 GHz, and the τ_f value was near zero (-12 ppm/°C), after sintering the sample at 1400 °C for 2 h with tiny $MnCO_3$ (5 mol%). Further Mn-substitution would deteriorate the microwave dielectric performance. In all, this study suggests that, substitution with magnetic ion of Mn^{2+} is a promising method both to promote the $Q \times f$ value and obtain near zero τ_f value of $ZnGa_2O_4$ ceramics.

Acknowledgement

The authors acknowledge the generous financial support from Priority Academic Program Development of Jiangsu Higher Education Institutions (PAPD), the Opening Project of the State Key Laboratory of High-Performance Ceramics and Superfine Microstructure (Project no. SKL201309SIC), the College Industrialization Project of Jiangsu Province (JHB2012-12), the Jiangsu Collaborative Innovation Center for Advanced Inorganic Function Composites, the Science and Technology Projects of Guangdong Province (Project no. 2011A091103002), and Graduate Student Training Innovation Project in Jiangsu Province (KYCX17_0973).

References

[1] W. Wersing, Microwave ceramics for resonator and filters, Curr. Opin. Solid. State Mater. Sci. 1 (1996) 715–731.
[2] R.J. Cava, Dielectric materials for applications in microwave communications, J. Mater. Chem. 11 (2000) 54–62.
[3] M.T. Sebastian, Dielectric materials for wireless communication, J. Mater. Chem. 11 (2010) 54–62.
[4] S.B. Narang, S. Bahel, Low loss dielectric ceramics for microwave applications: a review, J. Ceram. Process. Res. 11 (2010) 316–321.
[5] Z. Fu, P. Liu, J. Ma, X. Zhao, H. Zhang, Novel series of ultra-low loss microwave dielectric ceramics: $Li_2Mg_3BO_6$, (B = Ti, Sn, Zr), J. Eur. Ceram. Soc. 36 (2016) 625–629.
[6] Y.C. Chen, H.M. You, K.C. Chang, Influence of Li_2WO_4, aid and sintering temperature on microstructures and microwave dielectric properties of Zn_2SnO_4 ceramics, Ceram. Int. 41 (2014) 5257–5262.
[7] Y.C. Chen, Y.N. Wang, C.H. Hsu, Elucidating the dielectric properties of Mg_2SnO_4 ceramics at microwave frequency, J. Alloy. Compd. 509 (2011) 9650–9653.
[8] Y.C. Chen, H.M. You, Microwave dielectric properties of ZnO–B_2O_3–SiO_2-doped Zn_2SnO_4 ceramics for application in triple bands inverted-U shaped monopole antenna, J. Alloy. Compd. 616 (2014) 356–362.
[9] N.H. Nguyen, J.B. Lim, S. Nahm, et al., Effect of Zn/Si ratio on the microstructural and microwave dielectric properties of Zn_2SiO_4 ceramics, J. Am. Ceram. Soc. 90 (2007) 3127–3130.
[10] J.S. Kim, N.H. Nguyen, J.B. Lim, et al., Low-temperature sintering and microwave dielectric properties of the Zn_2SiO_4 ceramics, J. Am. Ceram. Soc. 91 (2008) 671–674.
[11] J.S. Kim, N.H. Nguyen, M.E. Song, et al., Effect of Bi_2O_3 addition on the sintering temperature and microwave dielectric properties of Zn_2SiO_4 ceramics, Int. J. Appl. Ceram. Tech. 6 (2009) 581–586.
[12] W. Lei, W.Z. Lu, J.H. Zhu, et al., Modification of $ZnAl_2O_4$ -based low-permittivity microwave dielectric ceramics by adding 2MO–TiO_2, (M = Co, Mg, and Mn), J. Am. Ceram. Soc. 91 (2008) 1958–1961.
[13] W. Lei, W.Z. Lu, D. Liu, et al., Phase evolution and microwave dielectric properties of $(1-x)ZnAl_2O_4 - xMg_2TiO_4$, ceramics, J. Am. Ceram. Soc. 92 (2009) 105–109.
[14] C.L. Huang, C.Y. Tai, C.Y. Huang, et al., Low-loss microwave dielectrics in the spinel-structured $(Mg_{1-x}Ni_x)Al_2O_4$ solid solutions, J. Am. Ceram. Soc. 93 (2010) 1999–2003.
[15] S. Takahashi, A. Kan, H. Ogawa, Microwave dielectric properties and crystal structures of spinel structured $MgAl_2O_4$ ceramics synthesized by a molten-salt method, J. Eur. Ceram. Soc. 37 (2016) 1001–1006.
[16] J. Xue, S. Wu, J. Li, Synthesis, microstructure, and microwave dielectric properties

of spinel $ZnGa_2O_4$ ceramics, J. Am. Ceram. Soc. 96 (2013) 2481–2485.
[17] M. Lu, O. Xin, S. Wu, et al., A facile hydrothermal route to self-assembled $ZnGa_2O_4$, particles and their microwave application, Appl. Surf. Sci. 364 (2016) 775–782.
[18] M.M. Can, G.H. Jaffari, S. Aksoy, et al., Synthesis and characterization of $ZnGa_2O_4$ particles prepared by solid state reaction, J. Alloy. Compd. 549 (2013) 303–307.
[19] S. Wu, J. Xue, R. Wang, et al., Synthesis, characterization and microwave dielectric properties of spinel $MgGa_2O_4$, ceramic materials, J. Alloy. Compd. 585 (2014) 542–548.
[20] A. Kan, T. Moriyama, S. Takahashi, et al., Cation distributions and microwave dielectric properties of spinel-structured $MgGa_2O_4$ ceramics, Jpn. J. Appl. Phys. 52 (2013) 09KH01.
[21] A. Kan, S. Takahashi, T. Moriyama, et al., Influence of Zn substitution for Mg on microwave dielectric properties of spinel-structured (1-x)$MgGa_2O_4$-x$ZnGa_2O_4$, Jpn. J. Appl. Phys. 53 (2014) 09PB03.
[22] S. Wu, J. Xue, Y. Fan, Spinel $Mg(Al,Ga)_2O_4$ solid solution as high-performance microwave dielectric ceramics, J. Am. Ceram. Soc. 97 (2014) 3555–3560.
[23] S. Takahashi, A. Kan, H. Ogawa, Microwave dielectric properties and cation distributions of $Zn_{1-3x}Al_{2+2x}O_4$ ceramics with defect structures, J. Eur. Ceram. Soc. 37 (2017) 3059–3064.
[24] X. Lu, W. Bian, Y. Li, et al., Influence of inverse spinel structured $CuGa_2O_4$ on microwave dielectric properties of normal spinel $ZnGa_2O_4$ ceramics, J. Am. Ceram. Soc. (2017), http://dx.doi.org/10.1111/jace.15264.
[25] S. Zhang, H. Sahin, E. Torun, et al., Fundamental mechanisms responsible for the temperature coefficient of resonant frequency in microwave dielectric ceramics, J. Am. Ceram. Soc. 100 (2017) 1508–1516.
[26] X.C. Fan, X.M. Chen, X.Q. Liu, Complex-permittivity measurement on high-Q materials via combined numerical approaches, IEEE. Trans. Microw. Theory 53 (2005) 3130–3134.
[27] R.J. Wiglusz, A. Watras, M. Malecka, et al., Structure evolution and up-conversion studies of ZnX^2O^4: Er^{3+}/Yb^{3+} (X = Al^{3+}, Ga^{3+}, In^{3+}) nanoparticles, Eur. J. Inorg. Chem. 6 (2014) 1090–1101.
[28] M.A. Laguna-Bercero, M.L. Sanjuan, R.I. Merino, Raman spectroscopic study of cation disorder in poly-and single crystals of the nickel aluminate spinel, J. Phys. Condens. Mater. 19 (2007) 186–217.
[29] V. Singh, R. Chakradhar, J. Rao, et al., Characterization, EPR and luminescence studies of ZnAl2O4:Mn phosphors, J. Lumin 128 (2008) 394–402.
[30] J. Liu, X. Duan, Y. Zhang, et al., Cation distribution and photoluminescence properties of Mn-doped $ZnGa_2O_4$, nanoparticles, J. Phys. Chem. Solids 81 (2015) 15–19.
[31] J. Popovic, B. Grzeta, B. Rakvin, et al., Partial inverse spinel structure of manganese-doped gahnite: XRD and EPR spectroscopy studies, J. Alloy. Compd. 509 (2011) 8487–8492.
[32] R.D. Shannon, Dielectric polarizabilities of ions in oxides and fluorides, J. Appl. Phys. 73 (1993) 348–366.